Time-resolved toxicity study reveals the dynamic interactions between uncoated silver nanoparticles and bacteria

Dong, Feng; Mohd Zaidi, Nurul Fitriah; Valsami-Jones, Eugenia; Kreft, Jan-Ulrich

DOI:
10.1080/17435390.2017.1342010

Document Version
Peer reviewed version

Citation for published version (Harvard):
Dong, F, Mohd Zaidi, NF, Valsami-Jones, E & Kreft, J-U 2017, 'Time-resolved toxicity study reveals the dynamic interactions between uncoated silver nanoparticles and bacteria', *Nanotoxicology*, pp. 1-10. https://doi.org/10.1080/17435390.2017.1342010

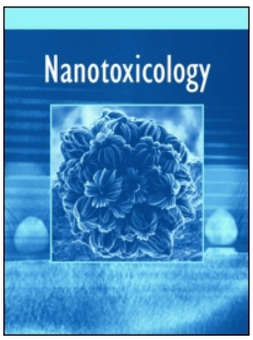

Nanotoxicology

ISSN: 1743-5390 (Print) 1743-5404 (Online) Journal homepage: http://www.tandfonline.com/loi/inan20

Time-resolved toxicity study reveals the dynamic interactions between uncoated silver nanoparticles and bacteria

Feng Dong, Nurul Fitriah Mohd Zaidi, Eugenia Valsami-Jones & Jan-Ulrich Kreft

To cite this article: Feng Dong, Nurul Fitriah Mohd Zaidi, Eugenia Valsami-Jones & Jan-Ulrich Kreft (2017): Time-resolved toxicity study reveals the dynamic interactions between uncoated silver nanoparticles and bacteria, Nanotoxicology, DOI: 10.1080/17435390.2017.1342010

To link to this article: http://dx.doi.org/10.1080/17435390.2017.1342010

Accepted author version posted online: 13 Jun 2017.

Time-resolved toxicity study reveals the dynamic interactions between uncoated silver nanoparticles and bacteria

Feng Dong[1], Nurul Fitriah Mohd Zaidi[1], Eugenia Valsami-Jones[2], Jan-Ulrich Kreft[1]

1 Institute of Microbiology and Infection & School of Biosciences, University of Birmingham, Edgbaston, Birmingham, B15 2TT, UK

2 School of Geography, Earth and Environmental Sciences, University of Birmingham, Edgbaston, Birmingham, B15 2TT, UK

Correspondence: Feng Dong, Institute of Microbiology and Infection, School of Biosciences, University of Birmingham, Edgbaston, Birmingham, B15 2TT, UK. Email: fengdongub@gmail.com; Present address: Nanyang Environment and Water Research Institute (NEWRI), Nanyang Technological University, Singapore 639798, Singapore

Time-resolved toxicity study reveals the dynamic interactions between uncoated silver nanoparticles and bacteria

It is still unclear whether the toxicity of silver nanoparticles (AgNPs) can be attributed solely to the release of Ag^+ or whether dissolved and nanoparticulate Ag act in parallel; this is due to the difficulty in distinguishing Ag^+- from AgNP-effects. Also, AgNPs undergo changes during toxicity tests. This is the first study to investigate the influence of AgNP dissolution over time on viable counts at high time resolution and low cell density, avoiding the apparently reduced toxicity at higher cell densities identified in our study. Uncapped AgNPs were synthesized to avoid any interference from surface coatings. The transformations of AgNPs during storage were reduced. Lowering the concentration of AgNPs reduced their aggregation in Davis minimal medium (DMM). Also, AgNPs dissolved more slowly in DMM than in water. The minimum inhibitory concentrations (MICs) of Ag^+ and AgNPs increased with cell density according to a power law, suggesting that binding to cells decreased effective concentrations. However, AgNPs acted as a reservoir of Ag, releasing new Ag^+ to maintain the Ag stress. The toxicity of AgNPs was dominated by dissolved Ag. Combining controlled conditions, high time-resolution and low cell density, we could demonstrate different roles of ionic and nano Ag in bacterial death caused by AgNPs.

Keywords: silver nanoparticles; toxicity; silver ions; dissolution; bacteria; antibacterial effects

Introduction

Silver (Ag) is not known to be required for any metabolic process, rather, it disturbs cellular metabolism and kills bacteria at low concentrations (Chernousova and Epple, 2013). By utilizing the high antimicrobial activity of Ag, silver nanoparticles (AgNPs) have become widely used nanomaterials in consumer products and medical applications (Chaloupka *et al.*, 2010), eventually leading to discharge into the natural environment (Gottschalk *et al.*, 2009, Pourzahedi and Eckelman, 2015). Along with the increasing use of AgNPs, their environmental implications are of special concern due to their high toxicity to microbes (Fabrega *et al.*, 2011, Kwak *et al.*, 2016).

Silver nanoparticles undergo various transformations upon exposure to various test media (Levard *et al.*, 2012, Petersen *et al.*, 2015). The large surface to volume ratio of AgNPs makes them highly reactive (Boles *et al.*, 2016). It is generally believed that the antibacterial activities of AgNPs are entirely due to the Ag^+ they release (Hsueh *et al.*, 2015) but the effects of ongoing Ag^+ release may differ from those of a Ag^+ pulse. Moreover, generation of reactive oxygen species (ROS) is another mechanism believed to be involved in nanoparticle toxicity in bacteria (Xu *et al.*, 2012, von Moos and Slaveykova, 2014). Silver nanoparticles can attach to bacterial surfaces or release Ag^+ into cells, inducing oxidative stress and disturb metabolism (Lok *et al.*, 2006), damage bacterial structures (Morones *et al.*, 2005, Auffan *et al.*, 2008) and kill cells (Choi and Hu, 2008, Joshi *et al.*, 2015).

The dissolution of AgNPs is highly dynamic and affected by nanoparticle properties such as surface coating and particle size (Ma *et al.*, 2012, Peretyazhko *et al.*, 2014), environmental conditions such as ionic strength (Chambers *et al.*, 2013), light (Gorham *et al.*, 2014), oxygen concentration (Kittler *et al.*, 2010, Loza *et al.*, 2014), temperature (Liu and Hurt, 2010), pH (Liu and Hurt, 2010, Fujiwara *et al.*, 2015) and chemical reactions at the nanoparticle surface (Liu *et al.*, 2010, Sotiriou *et al.*, 2012, Levard *et al.*, 2013). Ligands have been used to coat the surface of nanomaterials for functionalization or stabilization, which will affect their transformation and toxicity (Boles *et al.*, 2016). Positively-charged AgNPs might have stronger toxic effects on bacteria than negatively-charged AgNPs as a result of their higher tendency of attaching to the negatively-charged bacterial cell surface (El Badawy *et al.*, 2011). Sterically stabilized AgNPs are more stable than statically stabilized AgNPs in electrolyte solutions (El Badawy *et al.*, 2010) such as toxicological assay media (Tejamaya *et al.*, 2012). Silver nanoparticles also aggregate in natural waters but dissolved organic matter such as humic acids might stabilize AgNPs (Furtado *et al.*, 2015, Metreveli *et al.*, 2015). The extent of aggregation influences sedimentation rates (Lowry *et al.*, 2012, Furtado *et al.*, 2015), particle accessibility to cells (Cho *et al.*, 2011) and dissolution kinetics (He *et al.*, 2013). All these transformations combine to influence the toxicity of AgNPs. The variability in these dynamic transformations makes AgNP toxicity testing challenging. Thus, it is important to combine characterization of nanoparticles and their ongoing transformations with toxicity assays to improve the understanding of toxicity mechanisms. Real-time quantification of dissolution of AgNPs is critical to distinguish dissolved from nano Ag for toxicity tests. Besides, any differences in AgNP synthesis, storage and toxicity assay media compositions can also give rise to differences in results, hampering

comparability of studies (Petersen *et al.*, 2014).

In this study, the toxicity of AgNPs in the environmental model bacterium *Pseudomonas putida* was systematically and thoroughly investigated by combining many factors previously considered in isolation and monitoring the dynamic transformation of AgNPs and bacterial response at high time resolution under as well defined conditions as possible. Since AgNP effects largely arise from oxidation of the metallic silver under oxic conditions and ROS production only occurs when oxygen is present, we chose *P. putida*, an aerobic bacterium widespread in nature, to investigate the bacteria-AgNP interaction. It is an environmental model organism with well-known metabolism, stress responses and a high quality genome annotation (Nelson *et al.*, 2002, Belda *et al.*, 2016) and is versatile and able to survive in a variety of stressful environments. A citrate minimal medium was used to minimize potential changes of AgNPs during exposure to test media. Uncoated AgNPs were used to avoid interferences from surface ligands. They were stored under N_2 to reduce oxidation and ensure the consistency of primary AgNP dispersions. We not only investigated the toxicity of different concentrations of AgNPs but also examined the effect of bacterial cell density that is frequently ignored in standard toxicity tests. Indeed, we found that the apparent MICs increased with cell density according to a power law and as a consequence carried out toxicity assays at cell densities much lower than normal to avoid overestimating MICs. We also used lower doses of AgNPs (0-100 µg/L) than in most toxicity studies (0.1-100 mg/L) (Fabrega *et al.*, 2011) as these are closer to concentrations in the environment (<1 µg/L) (Keller and Lazareva, 2014) and typical for drinking water treatment (5-60 µg/L) (Sankar *et al.*, 2013). Using these more defined and appropriate conditions, we determined the dynamics of interactions of AgNP with bacteria by simultaneously following AgNP dissolution and

changes of viability at high time-resolution. We found that all or at least most of the bactericidal effect of AgNPs could be explained by the release of ionic silver from the nanoparticles. However, the effect of AgNPs differs from Ag^+ as AgNPs continuously release Ag^+ and thus maintain Ag^+ concentration, which should help to eradicate persisters.

Materials and methods

Synthesis of uncoated AgNPs

Uncoated AgNPs were synthesized by reducing silver nitrate ($AgNO_3$, Sigma-Aldrich) with sodium borohydride ($NaBH_4$, Sigma-Aldrich) at room temperature (19 ± 4 °C) (Polte *et al.*, 2012). We increased the $NaBH_4/AgNO_3$ concentration ratio from 6 to 25 to prevent aggregation during synthesis (Van Hyning *et al.*, 2001, Mulfinger *et al.*, 2007). All glassware for AgNPs synthesis and storage was soaked in 10% HNO_3, rinsed with deionized (DI) water and dried under ambient environment. The synthesized AgNPs were directly diluted to desired concentrations for aggregation, dissolution and toxicity tests.

Characterization of AgNPs

The localized surface plasmon resonance (LSPR) of uncoated AgNP suspensions was measured by UV-Vis absorption spectrometry (UV-Vis 6800, Jenway, Stone, UK). The hydrodynamic size of AgNPs was measured by dynamic light scattering (DLS) (Zetasizer Nano, Malvern Instruments, Malvern, UK) and differential centrifugal sedimentation (DCS) (DC24000, CPS Instruments, Oosterhout, Netherlands). Zeta potential was measured by Malvern Zetasizer Nano. The morphology of AgNPs was examined by transmission electron microscopy (TEM) (JEOL 1200EX, Tokyo, Japan). About 20 μL AgNP suspension was loaded on TEM grids (CF300-Cu Grids, Electron Microscopy Sciences, Hatfield, USA), followed by drying under ambient air.

To reduce the artificial aggregates, TEM grids were modified by 100 mg/L polylysine through loading 20 μL polylysine solutions (100 mg/L) on the grids for 1 h, rinsing with DI water and drying under ambient environment.

Storage of AgNP suspensions

The stability of AgNP stocks under ambient air (total Ag 25 mg/L) or nitrogen atmosphere (total Ag 2.3 mg/L) at 4 °C in the dark was compared by measuring the dissolved Ag concentration in these two atmospheres over 2–3 months by ultrafiltration (Amicon Ultra-15 Centrifugal Filter Unit 3 kDa, Merck Millipore, Watford, UK) at the centrifugal force of 4000 g for 30 min at 4 °C (Centrifuge 5804R, Eppendorf, Engelsdorf, Germany). Borohydride is not stable in H_2O, producing H_3BO_3 and $B(OH)_4^-$ (Van Hyning and Zukoski, 1998, Briggs, 2000). The major chemicals in the AgNP stocks were AgNPs, Ag^+, Na^+, H_3BO_3, $B(OH)_4^-$, and NO_3^-. For incubation under N_2, the bottle (100 or 250 mL, Duran) was flushed with large amounts of nitrogen gas for at least 5 min to minimize O_2 in the liquid and gas phase. The AgNP-N_2 stock was flushed again with N_2 and sealed as quickly as possible after every sample collection. To determine the total Ag concentration of AgNP stocks, the AgNP suspensions were digested by 70% HNO_3 (1 mL AgNP suspension was added into 9 mL HNO_3) overnight at room temperature. The mixture was then diluted to a final HNO_3 concentration of 0.2% (w/v) for graphite furnace atomic absorption spectrometry (GFAAS) (AAnalyst 600, PerkinElmer Instruments, USA). UV-Vis

absorption spectra and TEM morphologies of these two AgNP stocks were monitored during the long-term storage.

Aggregation of AgNPs in defined medium

The aggregation kinetics of AgNPs in a Davis minimal medium (DMM) was determined by real-time DLS and time-resolved UV-Vis absorption spectrometry. The hydrodynamic size changes of AgNPs in DMM salts solution (no citrate presents) were measured over 2 h. The increase of Z-average size measured by DLS indicates either aggregation or agglomeration of AgNPs as the method cannot distinguish the two (Sokolov *et al.*, 2015). Aggregates in the strict sense are clusters of irreversibly attached particles while and agglomerates are looser clusters of reversibly attached particles. Here, we use the term "aggregation" in a wider sense to encompass aggregation and agglomeration. The AgNP suspensions (0.5 mL, total Ag 100, 200 and 400 μg/L) were mixed with the same volume of DMM salts solution (pH 7.1) in disposable plastic (polystyrene) cuvettes, followed by immediate sample analysis. Temperature was controlled at 25 °C. The AgNP suspensions were obtained by diluting the stock (total Ag 2470 ± 183 μg/L, dissolved Ag 304 ± 10 μg/L, mean ± SD) with DI H_2O. The composition of DMM is as follows (per liter) (pH 7.2): 7.0 g K_2HPO_4, 2.0 g KH_2PO_4, 1.0 g $(NH_4)_2SO_4$, 0.1 g $MgSO_4$, 1.53 g sodium citrate dihydrate and 1 mL SL10 trace elements solution. The SL10 trace elements stock solution contains (per liter): 1500 mg $FeCl_2{\cdot}4H_2O$, 190 mg $CoCl_2{\cdot}6H_2O$, 100 mg

$MnCl_2 \cdot 4H_2O$, 70 mg $ZnCl_2$, 6 mg H_3BO_3, 36 mg $Na_2MoO_4 \cdot 2H_2O$, 24 mg $NiCl_2 \cdot 6H_2O$ and 2 mg $CuCl_2 \cdot 2H_2O$. Precipitation of silver with chloride, sulfate and phosphate in DMM salts solution can be neglected according to solubility calculations carried out with Visual MINTEQ (Version 3.0, The Royal Institute of Technology, Sweden) (Table S1).

Dissolution of AgNPs

The dissolution of AgNPs in DMM salts solution and H_2O was examined at 30 °C, the same temperature used for the toxicity tests. Silver nanoparticle suspensions (20 mL with 134, 328 or 730 μg/L) were mixed with the same volume of DMM salts solutions in 100 mL glass flasks, respectively. The glass flasks were cleaned in the following way: soaked in disinfectant (Virkon, Rely+On, DuPont) for 1 h, rinsed with tap water, washed with detergent, washed with Lanceracid (containing 20–50% acetic acid) (Lancer UK Ltd, Cambridge, UK), rinsed with distilled water, dried and sterilized at 160 °C for 2 h. To prevent settling of AgNPs, the flasks were shaken at the speed of 150 rpm. The change of concentration of dissolved Ag was quantified by a new combination of Ca^{2+} accelerated aggregation and centrifugation described by Dong *et al*. (2016). In brief, silver nanoparticles (0.5 mL) were aggregated by addition of the same volume of $Ca(NO_3)_2$ (2 mM) for 10 min and then settled down by centrifugation at 20,100 g for 30 min at room temperature (Centrifuge 5417 C, Eppendorf, Engelsdorf, Germany), leaving dissolved Ag in the supernatants. Supernatants (0.5

mL) were carefully collected and stored at -20 °C. To measure the Ag contents in the supernatants, the supernatants were digested by 1% HNO_3 at 80 °C for at least 12 h, further diluted to a final HNO_3 concentration of 0.2% (w/v), and measured by GFAAS. Each sample was measured in triplicate.

Adsorption of Ag^+ to the glass flasks under the same conditions was also examined. Silver ions solution (20 mL, 62 or 126 μg/L) was mixed with same volume of DMM salts solution or DI H_2O in 100 mL glass flasks with shaking at 120 rpm at 30 °C. Samples (1 mL) were collected over 96 h and stored at -20 °C. The Ag contents in these samples were measured in triplicate by GFAAS.

Bacterial strain and culture conditions

An environmental model bacterium *Pseudomonas putida* was chosen in this study. The green fluorescent protein (GFP) tagged derivative JB279 of *P. putida* KT2442 was generously donated by Prof. Søren Molin (Technical University of Denmark). A stable GFP is expressed from the strong LacI repressible promoter $P_{A1/04/03}$ that is part of the mini-Tn5-Km-T_1-T_0-gfpmut3*-$P_{A1/04/03}$ randomly inserted into the bacterial chromosome (Andersen *et al.*, 1998). Davis minimal medium (contain SL10 trace elements as described previously) supported growth at 30 °C. Low concentrations of borate (< 1.5 mM) were present in the AgNP stocks. Existing data on toxicity of borates to bacteria indicate that these low concentrations of borate, which were diluted more than 10 fold for actual toxicity assays, would be unlikely to cause

toxicity in *Pseudomonas putida* (Summers and Jacoby, 1978, Bringmann and Kühn, 1980).

Determination of MICs

The minimum inhibitory concentrations (MICs) of AgNPs and Ag^+ were determined according to a standard protocol (Andrews, 2001). The protocol was modified to study the influence of cell density on MICs by varying the initial cell numbers. Overnight cultures grew in 50 mL fresh DMM (contain 50 μg/L kanamycin) for 4–6 h to reach the mid-exponential phase. The culture was then diluted with fresh DMM to obtain different densities (10^4–10^8 CFU/mL). Within 30 min, 100 μL of the diluted culture was mixed with 100 μL different concentrations of AgNP suspensions or Ag^+ solution in a 96-microwell plate. Each treatment was conducted in triplicate. The plates were covered with lids and incubated at 30 °C for 16–24 h. Optical density (OD) was monitored to determine the MICs as the lowest concentrations that prevented growth (OD remain < 0.05).

AgNP and Ag^+ death kinetics

Death kinetics were determined by monitoring cell viability over 5 h at different concentrations of AgNPs or Ag^+. Low initial bacterial cell densities were chosen to avoid titration of AgNPs or Ag^+ by the biomass. Overnight cultures were diluted with fresh DMM and grown to mid-exponential phase as above, followed by dilution with DMM salts (no carbon source) to obtain final densities around 1×10^5 CFU/mL.

These diluted cultures (20 mL) were mixed with the same volumes of AgNP suspensions (0–100 μg/L) or Ag^+ solutions (0–50 μg/L) in 100 mL glass flasks. To prevent sedimentation of AgNPs, the cultures were shaken at 120 rpm at 30 °C. Plates for viable counts were immediately set up after taking samples rather than at the end of the 5 h experiment. The residual Ag^+/AgNPs will be diluted along with the dilution of the cell cultures for viable counting and further diluted into the agar, which will reduce any effects of residual AgNPs/Ag^+ on death kinetics.

Dissolved Ag contents in the culture treated by AgNPs were determined by the aggregation-centrifugation method described above. Two mM $Ca(NO_3)_2$ (0.5 mL) was added to cell culture (0.5 mL) to aggregate the AgNPs. The mixtures were then centrifuged (20,100 g, 30 min). The supernatants (0.5 mL) were collected and stored. The Ag contents in the supernatants were measured by GFAAS. For Ag^+-treated cultures, 1 mL cell culture was centrifuged (20,100 g, 30 min), and 0.5 mL supernatants were collected and stored at -20 °C.

Dose-responses were measured as above but with higher time resolution in order to obtain the death rates by linear regression of viable count versus time. The order of these treatments was randomized. Viable counts were examined by spreading 100 μL culture on LB plates at time 0, 10, 20, 30, 45 and 60 min.

Results

Synthesis, characterization and storage of uncoated AgNPs

Stable, uncoated AgNPs with round shape were obtained (Figure 1A). The characteristics of AgNP suspensions are listed in Table S2. Most of the AgNPs were in the size between 10 and 40 nm with an average diameter of 21 ± 11 nm (Figure 1B, Table S2). The zeta potential of AgNPs in H_2O (pH = 9.3 ± 0.4) was -40 ± 17 mV. The absorbance peak of the AgNP suspension was 394 ± 1 nm (Figure S1).

Uncapped AgNP suspension stored under ambient air slowly released Ag^+. The dissolved Ag concentration increased from 74 to 627 μg/L in three months. Under nitrogen atmosphere, in comparison, the dissolved Ag content in AgNP suspension did not change significantly (Figure 1C), confirmed by the lack of change of the UV-Vis absorption spectra (Figure S2). Compared to the transformations of AgNPs to large fused nanoparticles, nanobars and triangular shapes when exposed to air, the AgNPs stored under N_2 atmosphere changed little over 100 d (Figure S3), suggesting that storing AgNP suspensions in an anoxic environment ensures stability of AgNPs and should reduce variation between batches.

Aggregation and dissolution of AgNPs in a mineral medium

The hydrodynamic diameter and UV-Vis absorption spectra of AgNPs in DMM, a defined mineral medium for microbial growth, were measured over time to examine

the potential aggregation in the toxicity test media. Quicker aggregation leading to larger AgNP clusters was observed for higher concentrations of AgNPs in DMM salts solution (Figure 2A). The transformations of UV-Vis absorption spectra also demonstrated faster and more extensive aggregation of the AgNPs at the higher concentration by the quicker decrease of peak absorption, the larger red-shift of the LSPR band and the broadening of the UV-Vis absorption spectra (Figure S4).

Silver nanoparticles release Ag^+ into solution in oxic conditions. The dissolution kinetics of uncoated AgNPs in DMM salts solution and H_2O were recorded over 7 d (Figure 2B). Note that the rate of dissolution of AgNPs is size dependent so that the smaller AgNPs will dissolve faster than larger ones, making the rate of dissolution and size distribution time dependent. However, the duration of the experiments was sufficiently short to ensure the effect on dissolution rate was minimal. Silver nanoparticles dissolved 40-fold quicker in H_2O than in DMM salts solution (Table S3). In H_2O, half of the nano Ag dissolved in 1 d, followed by a slow Ag release over the next several days. A first-order dissolution kinetics model (p-value = 2.8×10^{-7}) revealed that the equilibrium dissolved Ag concentration was 232 ± 16 μg/L (value ± SE). It was calculated that 69% and 13% of the nano Ag were dissolved for 365 μg/L AgNPs in H_2O and DMM salts solution within 7 d, respectively.

The salts in the medium might reduce Ag dissolution but cannot prevent Ag^+ adsorption (Figure 2C); therefore, silver sorption to culture vessels cannot be

excluded under our experimental conditions. The chemical properties of solutes in the medium and the vessel geometry, surface chemistry and material all affect Ag^+ sorption (West *et al.*, 1966, Struempler, 1973, Malysheva *et al.*, 2015, Sekine *et al.*, 2015). However, sorption of Ag to the surface of the microwells can probably be neglected since already 4.5 µg/L of Ag^+ completely inhibited growth at the low cell density of 1.2×10^4 CFU/mL while the same number of cells grew to a high density in Ag-free control condition. While we did not quantify Ag sorption, we measured the actual concentrations of dissolved Ag in the media.

Effect of cell density on inhibition

In the standard protocol for determination of MICs, cell cultures are grown into the exponential phase to reach a cell density of 1×10^6 CFU/mL (Andrews, 2001). In this study, MICs of AgNPs and Ag^+ were examined at various initial bacterial densities. *P. putida* was more susceptible to Ag^+ than to AgNPs by more than one order of magnitude (Figure 3). Interestingly, the dependence of the MICs of Ag^+ and AgNPs for *P. putida* on initial cell densities followed a power law with an exponent of about 0.4. This means that the increase of MIC with cell density is sub-linear and therefore dividing the MIC by cell density to express MIC in terms of Ag/cell rather than Ag/volume will lead to a negative exponent of the power law of about -0.6. It is conceivable that Ag can 'recycle' and hit targets more than once or that it is more likely to hit a cell at higher cell density but we currently have no evidence for this so

such explanations remain speculative. Both MICs increased by about one order of magnitude when the initial cell density increased by three orders of magnitude, from 10^4 to 10^7 CFU/mL (Figure 3). The dissolution of AgNPs can occur during incubation of the cells. As it was not feasible to measure dissolved Ag concentrations over time in 96-well plates during the MIC tests, flasks with larger culture volumes were used for determining toxicity kinetics.

Inhibition kinetics

Viable cell counts and dissolved Ag concentrations were monitored over time to determine the inhibition kinetics for Ag^+ or AgNPs. Figure 4A and B show that Ag^+ and AgNPs killed the cells during the first 1–2 h at this low initial cell density of about 5000 CFU/mL. Treatment with 30 μg/L of Ag^+ killed all cells within 1 h but most cells survived treatment with 5 and 10 μg/L of Ag^+ for 5 h (Figure 4A). Several hundred cells/mL survived 20 μg/L of Ag^+ for 5 h. Interestingly, the populations treated with 5, 10, and 20 μg/L Ag^+ recovered to a similarly large population density during prolonged exposure (72 h), but not at 30 μg/L of Ag^+ (Table 1). The dissolved Ag concentrations showed a parallel decline with cell viability (Figure 4C). Under the treatment with 5, 10, and 20 μg/L of Ag^+, the dissolved Ag concentrations decreased to less than 1.2 μg/L within 2 h (Figure 4C) and to undetectable levels after 72 h (Table 1). In contrast, relatively high concentrations of residual Ag^+ (6.5–9 μg/L) remained in the culture treated with 30 μg/L of Ag^+. Presumably this was why all cells

were killed at this concentration (Figure 4C, Table 1).

Toxicity of AgNPs was lower than that of Ag^+. At 10 μg/L, growth was similar to the control (Figure 4B). Higher concentrations of AgNPs caused quick bacterial death. Around 50 cells/mL survived treatment with 20 μg/L AgNPs. All cells were eradicated by 50 and 100 μg/L AgNPs within 5 h. The decline of dissolved Ag was similar to the decline of cell viability. After 72 h, no regrowth occurred at 50 and 100 μg/L AgNPs, but large populations were obtained at lower concentrations (Table 1). The initial dissolved Ag^+ concentration in the 50 μg/L AgNP treatment was 18 μg/L. Regrowth would be expected at this concentration of dissolved Ag based on the Ag^+ inhibition kinetics (Table 1). However, continuing dissolution of AgNPs released new Ag^+ into the culture (Figure 4D). The dissolution rates for 50 and 100 μg/L AgNP suspensions in the diluted bacterial culture were $(5.7 \pm 0.4) \times 10^{-2}$ and $(3.3 \pm 0.3) \times 10^{-2}$ μg Ag/(μg AgNP·h) within 1.5–5.5 h, respectively, sufficient to completely eradicate the bacteria in the long term (Table 1). At low concentrations of AgNPs (10 and 20 μg/L), dissolution was too limited to kill the cells, allowing regrowth.

Quantifying the toxicity of Ag^+ and AgNPs

Since most of the change in cell viability happened very quickly (Figure 4), the inhibition kinetics were monitored with higher time resolution (Figure 5A and B). The number of cells at the start of the experiment varied somewhat, which may explain why fewer cells, 3 rather than 680 CFU/mL, survived at 10 than at 15 μg/L of Ag^+ (Figure 5A). Therefore, the toxicity in terms of death rate was quantified by linear regression of cell viability against time. The death rates gradually increased from about 0 to 86 ± 17 CFU/(mL·min) (slope ± SE) when Ag^+ concentrations increased from 0 to 32 μg/L (Figure 5C). A further increase to 40 μg/L did not significantly increase toxicity. The highest death rate under the treatment of AgNPs was somewhat lower, 64 ± 7 CFU/(mL·min), at the higher concentration of 80 μg/L, confirming stronger toxicity of Ag^+ in *P. putida* than AgNPs. Assuming that the toxicity of AgNPs is solely due to dissolved Ag, the toxicity of AgNPs can be expressed in terms of dissolved Ag. As expected, the AgNP death rates in terms of dissolved Ag were closer to the death rates for Ag^+ (Figure 5C). There was no significant difference in the specific death rates for Ag^+ and dissolved Ag in AgNP suspension (Figure 5D, Table S4). This suggested that the toxicity of AgNPs was mainly due to dissolved Ag.

Discussion

This study investigated the dynamic interactions between AgNPs and bacteria in well–defined conditions in minimal medium using uncoated AgNPs and monitoring viable counts and dissolved Ag^+ at high time resolution. We examined transformations of AgNPs in toxicity test media and how the dissolution of AgNPs affects their toxicity in bacteria over time, demonstrating the dynamic antibacterial effects in response to nanomaterial transformations.

Uncoated AgNPs were synthesized with an increasedBH_4^-/Ag^+ concentration ratio. Storing the AgNP stock in nitrogen atmosphere achieved long-term stability of AgNPs. There are two steps involved in the dissolution of AgNPs: (1) oxidation of AgNPs, forming Ag_xO_y on the surface of the nanoparticle; (2) hydrolysis of the Ag_xO_y layer in H_2O, resulting in Ag^+ release into the surrounding liquid (Zhang *et al.*, 2015). Oxidation of AgNPs was prevented in N_2, thereby avoiding dissolution.

Higher AgNP concentrations favor aggregation by increasing the chances of effective collisions that enable nanoparticles to overcome the energy barrier to form aggregates (Huynh and Chen, 2011, Zhang *et al.*, 2012). The relatively small changes of hydrodynamic size and stable UV-Vis absorption spectra suggested that low concentrations of AgNPs (50 µg/L) were relatively stable in DMM. Sedimentation of AgNPs in cultures or assays was not observed and not likely to take place in this study since the aggregates were not large enough to settle rapidly (Cho *et al.*, 2011,

Alexander *et al.*, 2013).

Silver nanoparticles spontaneously dissolve in the presence of oxygen in biological media. Their aggregation status and surface modification might affect the slow dissolution of uncoated AgNPs in DMM. Aggregates of nanoparticles have fewer active sites on their surface, which reduces oxidation and dissolution (He *et al.*, 2013). This could explain the higher dissolution rate at lower AgNP concentrations (Table S3) as they would have a lower degree of aggregation. However, this aggregation effect is unlikely to be sufficient to explain the decrease of dissolution rates by two orders of magnitude since the aggregation at low concentrations of AgNPs in DMM was not strong (Figure 2A). Instead, the much reduced AgNP dissolution in DMM suggests that the chemicals in the medium not only affect aggregation but also govern the dissolution kinetics of AgNPs. Chloride (Cl^- in DMM is 0.95×10^{-2} mM) might form complexes with Ag on the surface of the AgNPs, decreasing the dissolution rate (Levard *et al.*, 2013). Additionally, phosphate or sulfate may also decrease the surface activity of AgNPs. A similar, rapid Zn^{2+} release in H_2O but slow dissolution in phosphate solution has been reported for ZnO nanoparticles as a result of phosphate reacting with the particle surface (Lv *et al.*, 2012). Given the high concentrations of phosphate (55 mM) and sulfate (8.4 mM) in DMM, Ag_3PO_4 or Ag_2SO_4 complexes might have formed on the surface of AgNPs, slowing down Ag^+ release.

As we observed, Ag^+ was more toxic in *P. putida* than AgNPs. The MICs for Ag^+ and AgNPs were dependent on initial cell densities. By varying cell density over four orders of magnitude, we could observe a power law relationship between MICs and cell density. A dependence on cell density has been previously observed with antibiotics (Udekwu *et al.*, 2009) and can be simulated via a direct antibiotic-biomolecule reaction (Abel zur Wiesch *et al.*, 2015). Compared to essential cellular metals (e.g., K, Zn, Fe and Mg), Ag has a higher affinity to various biomolecules, especially those containing thiol groups (Eckhardt *et al.*, 2013, Lemire *et al.*, 2013). It is therefore expected that bacterial components complex Ag (Vijayaraghavan and Yun, 2008, Lemire *et al.*, 2013). The interactions between Ag and bacteria can be understood as metal-cell complexation while leading to the chelation of free Ag (Wakshlak *et al.*, 2015). The cell density effect is likely due to titration of Ag by the biomass. The higher the bacterial density, the larger the fraction of Ag that will be sequestered by the inhibited or dead cells. This lowering of the active concentration of Ag reduces apparent Ag toxicity. Therefore, to avoid this overestimation of MICs, we used a low cell density of about 5,000 CFU/mL for toxicity assays as a default.

Simultaneous decline of dissolved Ag concentration accompanied bacterial cell death. The decrease of concentrations of dissolved Ag in Ag^+-treated and AgNP-treated cultures might be attributed to the Ag titration by bacterial cells and the sorption of Ag to the flask surface. Some bacteria can survive long exposures to Ag^+ or AgNPs and the population can subsequently regrow, suggesting the presence of persisters resistant

to low concentrations of Ag (Brauner *et al.*, 2016). At higher initial concentrations of Ag^+ or AgNPs, there will still be enough Ag^+ left to kill any persisters, explaining the absence of regrowth at high Ag concentrations. For AgNPs, toxicity effects are complicated by the continuous dissolution of AgNPs replenishing dissolved Ag, which would be an advantage for killing persisters.

Since AgNPs are not toxic under anoxic conditions, which prevent their dissolution, it has been suggested that all AgNP effects are indirect, due to the Ag^+ they release under oxic conditions (Xiu *et al.*, 2012). However, under oxic conditions, AgNPs enhance the generation of ROS, which would constitute a nanoparticle-specific effect separate from dissolution (Auffan *et al.*, 2008, Xu *et al.*, 2012, von Moos *et al.*, 2014, Joshi *et al.*, 2015). Uptake of AgNPs would constitute another NP-specific effect. Several electron microscopic observations of AgNPs inside bacterial cells have been made, however, the uptake mechanism remains unclear since bacteria do not have an endocytosis pathway. It seems most likely that AgNPs enter the cell after the membrane has become damaged (von Moos *et al.*, 2014). The apparently internalized AgNPs could also be the result of artefacts from sample preparation. Moreover, AgNPs could form inside the cell *de novo* by the reduction of intracellular Ag^+ after uptake of dissolved Ag^+ (Klaus *et al.*, 1999, Wakshlak *et al.*, 2015). Developing a method for measuring intracellular Ag^+ concentrations has enabled the demonstration that the intracellular concentration is sufficient to explain the rate of bacterial death (Bondarenko *et al.*, 2013). Note that this is not necessarily an argument against

AgNP-specific effects as larger concentrations of Ag^+ accumulate on the surface of AgNPs compared to the concentration of Ag^+ ions in the homogeneous bulk liquid (Pfeiffer *et al.*, 2014). Therefore, AgNPs trapped by the cell wall could deliver higher concentrations of Ag^+ at the cell surface, which could enhance the toxic effects of AgNPs. Moreover, unlike dissolved silver, nanoparticles could function as a silver reservoir that can sustain the continued release of Ag^+. Our results suggest that the concentration of dissolved Ag that is maintained in AgNP suspensions is sufficient to explain most of the bactericidal effects of AgNPs (Figure 5d).

Conclusions

In this study, the time-resolved transformations of AgNPs in a microbial medium were captured and the bacterial viability was directly quantified, revealing the dynamic interactions between AgNPs and bacteria, which have important implications for application and environmental risk assessment of AgNPs. We used well-defined conditions such as minimal media and uncapped AgNPs and stored AgNPs under nitrogen to increase stability. Sufficient time resolution enabled us to capture the rapid initial changes. Our results suggest that the aggregation of AgNPs in the environment might be limited since diluting AgNPs to lower concentrations reduced their aggregation rate in electrolyte solutions. We showed that oxygen, salts in the medium and aggregation status influenced the release of Ag^+ from AgNPs, suggesting that dissolution kinetics differ in different natural environments such as soil, freshwater and ocean. An anoxic environment or the presence of salts slowed down the dissolution of AgNPs. Considering the huge range of exposure conditions, the toxicity of AgNPs should be evaluated based on the Ag^+ release kinetics in the given environment. We demonstrated that the toxic effects depend not only on the concentrations of Ag^+ and AgNPs but also on the density of cells, which could be described by a power law with an exponent of about 0.4, that is, a sub-linear increase of MIC with cell density. This suggests that low levels of AgNPs, considered to be non-toxic, may well be toxic for more dilute bacterial communities, typical of most habitats. Hence, we used the low bacterial density of about 5,000 CFU/mL for the

toxicity assays in contrast to the standard 5×10^5 CFU/mL. While the biomass titrates AgNPs and/or Ag^+, reducing the effective concentration of Ag surrounding individual bacteria if there are many, AgNPs continuously release Ag^+ to replenish dissolved Ag in oxic environments, facilitating long-term inhibition. Comparing the bacterial death rates due to AgNPs and Ag^+ showed that the bactericidal activities of AgNPs could be mostly attributed to the concentrations of dissolved Ag we simultaneously measured in the AgNP suspensions. However, the sustained release of Ag^+ from AgNPs can still make an important difference, e.g. in eradicating persister cells.

Acknowledgements

We are grateful for a studentship from the Darwin Trust Edinburgh for Feng Dong and support from NERC via the Facility for Environmental Nanoscience Analysis and Characterisation (FENAC) at the University of Birmingham.

Declaration of interest

No potential conflict of interest was reported by the authors.

References

Abel Zur Wiesch, P., Abel, S., Gkotzis, S., Ocampo, P., Engelstädter, J., Hinkley, T., Magnus, C., Waldor, M.K., Udekwu, K. & Cohen, T., 2015. Classic reaction kinetics can explain complex patterns of antibiotic action. *Science Translational Medicine,* 7**,** 287ra73-287ra73.

Alexander, C.M., Dabrowiak, J.C. & Goodisman, J., 2013. Gravitational sedimentation of gold nanoparticles. *Journal of Colloid and Interface Science,* 396**,** 53-62.

Andersen, J.B., Sternberg, C., Poulsen, L.K., Bjorn, S.P., Givskov, M. & Molin, S., 1998. New unstable variants of green fluorescent protein for studies of transient gene expression in bacteria. *Applied and Environmental Microbiology,* 64**,** 2240-2246.

Andrews, J.M., 2001. Determination of minimum inhibitory concentrations. *Journal of Antimicrobial Chemotherapy,* 48**,** 5-16.

Auffan, M., Achouak, W., Rose, J., Roncato, M.-A., Chanéac, C., Waite, D.T., Masion, A., Woicik, J.C., Wiesner, M.R. & Bottero, J.-Y., 2008. Relation between the redox state of iron-based nanoparticles and their cytotoxicity toward *Escherichia coli*. *Environmental Science & Technology,* 42**,** 6730-6735.

Belda, E., Van Heck, R.G.A., Lopez-Sanchez, M.J., Cruveiller, S., Barbe, V., Fraser, C., Klenk, H.-P., Petersen, J., Morgat, A., Nikel, P.I., Vallenet, D., Rouy, Z., Sekowska, A., Martins Dos Santos, V.a.P., De Lorenzo, V., Danchin, A. & Médigue, C., 2016. The revisited genome of *Pseudomonas putida* KT2440 enlightens its value as a robust metabolic chassis. *Environmental Microbiology*, n/a-n/a.

Boles, M.A., Ling, D., Hyeon, T. & Talapin, D.V., 2016. The surface science of nanocrystals. *Nat Mater,* 15**,** 141-153.

Bondarenko, O., Ivask, A., Käkinen, A., Kurvet, I. & Kahru, A., 2013. Particle-cell contact enhances antibacterial activity of silver nanoparticles. *Plos ONE,* 8**,** e64060.

Brauner, A., Fridman, O., Gefen, O. & Balaban, N.Q., 2016. Distinguishing between resistance, tolerance and persistence to antibiotic treatment. *Nat Rev Micro,* 14**,** 320-330.

Briggs, M., 2000. Boron oxides, boric acid, and borates. *Kirk-Othmer Encyclopedia of*

Chemical Technology. John Wiley & Sons, Inc.

Bringmann, G. & Kühn, R., 1980. Comparison of the toxicity thresholds of water pollutants to bacteria, algae, and protozoa in the cell multiplication inhibition test. *Water Research,* 14**,** 231-241.

Chaloupka, K., Malam, Y. & Seifalian, A.M., 2010. Nanosilver as a new generation of nanoproduct in biomedical applications. *Trends in Biotechnology,* 28**,** 580-588.

Chambers, B.A., Afrooz, A.R.M.N., Bae, S., Aich, N., Katz, L., Saleh, N.B. & Kirisits, M.J., 2013. Effects of chloride and ionic strength on physical morphology, dissolution, and bacterial toxicity of silver nanoparticles. *Environmental Science & Technology,* 48**,** 761-769.

Chernousova, S. & Epple, M., 2013. Silver as antibacterial agent: ion, nanoparticle, and metal. *Angewandte Chemie-International Edition,* 52**,** 1636-1653.

Cho, E.C., Zhang, Q. & Xia, Y.N., 2011. The effect of sedimentation and diffusion on cellular uptake of gold nanoparticles. *Nature Nanotechnology,* 6**,** 385-391.

Choi, O. & Hu, Z., 2008. Size dependent and reactive oxygen species related nanosilver toxicity to nitrifying bacteria. *Environmental Science & Technology,* 42**,** 4583-4588.

Dong, F., Valsami-Jones, E. & Kreft, J.-U., 2016. New, rapid method to measure dissolved silver concentration in silver nanoparticle suspensions by aggregation combined with centrifugation. *Journal of Nanoparticle Research,* 18**,** 1-12.

Eckhardt, S., Brunetto, P.S., Gagnon, J., Priebe, M., Giese, B. & Fromm, K.M., 2013. Nanobio silver: its interactions with peptides and bacteria, and its uses in medicine. *Chemical Reviews*.

El Badawy, A.M., Luxton, T.P., Silva, R.G., Scheckel, K.G., Suidan, M.T. & Tolaymat, T.M., 2010. Impact of environmental conditions (pH, ionic strength, and electrolyte type) on the surface charge and aggregation of silver nanoparticles suspensions. *Environmental Science & Technology,* 44**,** 1260-1266.

El Badawy, A.M., Silva, R.G., Morris, B., Scheckel, K.G., Suidan, M.T. & Tolaymat, T.M., 2011. Surface charge-dependent toxicity of silver nanoparticles. *Environmental Science & Technology,* 45**,** 283-287.

Fabrega, J., Luoma, S.N., Tyler, C.R., Galloway, T.S. & Lead, J.R., 2011. Silver nanoparticles: Behaviour and effects in the aquatic environment. *Environment*

International, 37**,** 517-531.

Fujiwara, K., Sotiriou, G.A. & Pratsinis, S.E., 2015. Enhanced Ag^{+} ion release from aqueous nanosilver suspensions by absorption of ambient CO2. *Langmuir,* 31**,** 5284-5290.

Furtado, L.M., Norman, B.C., Xenopoulos, M.A., Frost, P.C., Metcalfe, C.D. & Hintelmann, H., 2015. Environmental fate of silver nanoparticles in Boreal Lake ecosystems. *Environmental Science & Technology,* 49**,** 8441-8450.

Gorham, J., Rohlfing, A., Lippa, K., Maccuspie, R., Hemmati, A. & David Holbrook, R., 2014. Storage wars: how citrate-capped silver nanoparticle suspensions are affected by not-so-trivial decisions. *Journal of Nanoparticle Research,* 16**,** 1-14.

Gottschalk, F., Sonderer, T., Scholz, R.W. & Nowack, B., 2009. Modeled environmental concentrations of engineered nanomaterials (TiO2, ZnO, Ag, CNT, Fullerenes) for different regions. *Environmental Science & Technology,* 43**,** 9216-9222.

He, D., Bligh, M.W. & Waite, T.D., 2013. Effects of aggregate structure on the dissolution kinetics of citrate-stabilized silver nanoparticles. *Environmental Science & Technology,* 47**,** 9148-9156.

Hsueh, Y.-H., Lin, K.-S., Ke, W.-J., Hsieh, C.-T., Chiang, C.-L., Tzou, D.-Y. & Liu, S.-T., 2015. The antimicrobial properties of silver nanoparticles in *Bacillus subtilis* are mediated by released Ag^{+} ions. *PLoS ONE,* 10**,** e0144306.

Huynh, K.A. & Chen, K.L., 2011. Aggregation kinetics of citrate and polyvinylpyrrolidone coated silver nanoparticles in monovalent and divalent electrolyte solutions. *Environmental Science & Technology,* 45**,** 5564-5571.

Joshi, N., Ngwenya, B.T., Butler, I.B. & French, C.E., 2015. Use of bioreporters and deletion mutants reveals ionic silver and ROS to be equally important in silver nanotoxicity. *Journal of Hazardous Materials,* 287**,** 51-58.

Keller, A.A. & Lazareva, A., 2014. Predicted releases of engineered nanomaterials: from global to regional to local. *Environmental Science & Technology Letters,* 1**,** 65-70.

Kittler, S., Greulich, C., Diendorf, J., Köller, M. & Epple, M., 2010. Toxicity of silver nanoparticles increases during storage because of slow dissolution under release of silver ions. *Chemistry of Materials,* 22**,** 4548-4554.

Klaus, T., Joerger, R., Olsson, E. & Granqvist, C.G., 1999. Silver-based crystalline

nanoparticles, microbially fabricated. *Proceedings of the National Academy of Sciences of the United States of America,* 96**,** 13611-13614.

Kwak, J.I., Cui, R., Nam, S.-H., Kim, S.W., Chae, Y. & An, Y.-J., 2016. Multispecies toxicity test for silver nanoparticles to derive hazardous concentration based on species sensitivity distribution for the protection of aquatic ecosystems. *Nanotoxicology,* 10**,** 521-530.

Lemire, J.A., Harrison, J.J. & Turner, R.J., 2013. Antimicrobial activity of metals: mechanisms, molecular targets and applications. *Nature Reviews Microbiology,* 11**,** 371-384.

Levard, C., Hotze, E.M., Lowry, G.V. & Brown, G.E., 2012. Environmental transformations of silver nanoparticles: impact on stability and toxicity. *Environmental Science & Technology,* 46**,** 6900-6914.

Levard, C., Mitra, S., Yang, T., Jew, A.D., Badireddy, A.R., Lowry, G.V. & Brown, G.E., 2013. Effect of chloride on the dissolution rate of silver nanoparticles and toxicity to *E. coli*. *Environmental Science & Technology,* 47**,** 5738-5745.

Liu, J. & Hurt, R.H., 2010. Ion release kinetics and particle persistence in aqueous nano-silver colloids. *Environmental Science & Technology,* 44**,** 2169-2175.

Liu, J., Sonshine, D.A., Shervani, S. & Hurt, R.H., 2010. Controlled release of biologically active silver from nanosilver surfaces. *Acs Nano,* 4**,** 6903-6913.

Lok, C.N., Ho, C.M., Chen, R., He, Q.Y., Yu, W.Y., Sun, H.Z., Tam, P.K.H., Chiu, J.F. & Che, C.M., 2006. Proteomic analysis of the mode of antibacterial action of silver nanoparticles. *Journal of Proteome Research,* 5**,** 916-924.

Lowry, G.V., Espinasse, B.P., Badireddy, A.R., Richardson, C.J., Reinsch, B.C., Bryant, L.D., Bone, A.J., Deonarine, A., Chae, S., Therezien, M., Colman, B.P., Hsu-Kim, H., Bernhardt, E.S., Matson, C.W. & Wiesner, M.R., 2012. Long-term transformation and fate of manufactured Ag nanoparticles in a simulated large scale freshwater emergent wetland. *Environmental Science & Technology,* 46**,** 7027-7036.

Loza, K., Diendorf, J., Sengstock, C., Ruiz-Gonzalez, L., Gonzalez-Calbet, J.M., Vallet-Regi, M., Koller, M. & Epple, M., 2014. The dissolution and biological effects of silver nanoparticles in biological media. *Journal of Materials Chemistry B,* 2**,** 1634-1643.

Lv, J., Zhang, S., Luo, L., Han, W., Zhang, J., Yang, K. & Christie, P., 2012. Dissolution and microstructural transformation of ZnO nanoparticles under the influence of phosphate. *Environmental Science & Technology,* 46**,** 7215-7221.

Ma, R., Levard, C., Marinakos, S.M., Cheng, Y.W., Liu, J., Michel, F.M., Brown, G.E. & Lowry, G.V., 2012. Size-controlled dissolution of organic-coated silver nanoparticles. *Environmental Science & Technology,* 46**,** 752-759.

Malysheva, A., Ivask, A., Hager, C., Brunetti, G., Marzouk, E.R., Lombi, E. & Voelcker, N.H., 2015. Sorption of silver nanoparticles to laboratory plastic during (eco)toxicological testing. *Nanotoxicology***,** 1-6.

Metreveli, G., Philippe, A. & Schaumann, G.E., 2015. Disaggregation of silver nanoparticle homoaggregates in a river water matrix. *Science of the Total Environment,* 535**,** 35-44.

Morones, J.R., Elechiguerra, J.L., Camacho, A., Holt, K., Kouri, J.B., Ramirez, J.T. & Yacaman, M.J., 2005. The bactericidal effect of silver nanoparticles. *Nanotechnology,* 16**,** 2346-2353.

Mulfinger, L., Solomon, S.D., Bahadory, M., Jeyarajasingam, A.V., Rutkowsky, S.A. & Boritz, C., 2007. Synthesis and study of silver nanoparticles. *Journal of Chemical Education,* 84**,** 322-325.

Nelson, K.E., Weinel, C., Paulsen, I.T., Dodson, R.J., Hilbert, H., Martins Dos Santos, V.a.P., Fouts, D.E., Gill, S.R., Pop, M., Holmes, M., Brinkac, L., Beanan, M., Deboy, R.T., Daugherty, S., Kolonay, J., Madupu, R., Nelson, W., White, O., Peterson, J., Khouri, H., Hance, I., Lee, P.C., Holtzapple, E., Scanlan, D., Tran, K., Moazzez, A., Utterback, T., Rizzo, M., Lee, K., Kosack, D., Moestl, D., Wedler, H., Lauber, J., Stjepandic, D., Hoheisel, J., Straetz, M., Heim, S., Kiewitz, C., Eisen, J., Timmis, K.N., Düsterhöft, A., Tümmler, B. & Fraser, C.M., 2002. Complete genome sequence and comparative analysis of the metabolically versatile *Pseudomonas putida* KT2440. *Environmental Microbiology,* 4**,** 799-808.

Peretyazhko, T.S., Zhang, Q. & Colvin, V.L., 2014. Size-controlled dissolution of silver nanoparticles at neutral and acidic pH conditions: kinetics and size changes. *Environmental Science & Technology,* 48**,** 11954-11961.

Petersen, E.J., Diamond, S.A., Kennedy, A.J., Goss, G.G., Ho, K., Lead, J., Hanna, S.K., Hartmann, N.B., Hund-Rinke, K., Mader, B., Manier, N., Pandard, P., Salinas, E.R. & Sayre, P., 2015. Adapting OECD aquatic toxicity tests for use with manufactured nanomaterials: key issues and consensus recommendations. *Environmental Science & Technology,* 49**,** 9532-9547.

Petersen, E.J., Henry, T.B., Zhao, J., Maccuspie, R.I., Kirschling, T.L., Dobrovolskaia, M.A., Hackley, V., Xing, B. & White, J.C., 2014. Identification and avoidance of potential artifacts and misinterpretations in nanomaterial ecotoxicity

measurements. *Environmental Science & Technology,* 48**,** 4226-4246.

Pfeiffer, C., Rehbock, C., Hühn, D., Carrillo-Carrion, C., De Aberasturi, D.J., Merk, V., Barcikowski, S. & Parak, W.J., 2014. Interaction of colloidal nanoparticles with their local environment: the (ionic) nanoenvironment around nanoparticles is different from bulk and determines the physico-chemical properties of the nanoparticles. *Journal of The Royal Society Interface,* 11.

Polte, J., Tuaev, X., Wuithschick, M., Fischer, A., Thuenemann, A.F., Rademann, K., Kraehnert, R. & Emmerling, F., 2012. Formation mechanism of colloidal silver nanoparticles: analogies and differences to the growth of gold nanoparticles. *Acs Nano,* 6**,** 5791-5802.

Pourzahedi, L. & Eckelman, M.J., 2015. Environmental life cycle assessment of nanosilver-enabled bandages. *Environmental Science & Technology,* 49**,** 361-368.

Sankar, M.U., Aigal, S., Maliyekkal, S.M., Chaudhary, A., Anshup, Kumar, A.A., Chaudhari, K. & Pradeep, T., 2013. Biopolymer-reinforced synthetic granular nanocomposites for affordable point-of-use water purification. *Proceedings of the National Academy of Sciences,* 110**,** 8459-8464.

Schneider, C.A., Rasband, W.S. & Eliceiri, K.W., 2012. NIH Image to ImageJ: 25 years of image analysis. *Nat Meth,* 9**,** 671-675.

Sekine, R., Khurana, K., Vasilev, K., Lombi, E. & Donner, E., 2015. Quantifying the adsorption of ionic silver and functionalized nanoparticles during ecotoxicity testing: test container effects and recommendations. *Nanotoxicology,* 9**,** 1005-1012.

Sokolov, S.V., Tschulik, K., Batchelor-Mcauley, C., Jurkschat, K. & Compton, R.G., 2015. Reversible or not? Distinguishing agglomeration and aggregation at the nanoscale. *Analytical Chemistry,* 87**,** 10033-10039.

Sotiriou, G.A., Meyer, A., Knijnenburg, J.T.N., Panke, S. & Pratsinis, S.E., 2012. Quantifying the origin of released Ag^+ ions from nanosilver. *Langmuir,* 28**,** 15929-15936.

Struempler, A.W., 1973. Adsorption characteristics of silver, lead, cadmium, zinc, and nickel on borosilicate glass, polyethylene, and polypropylene container surfaces. *Analytical Chemistry,* 45**,** 2251-2254.

Summers, A.O. & Jacoby, G.A., 1978. Plasmid-determined resistance to boron and chromium compounds in pseudomonas aeruginosa. *Antimicrobial Agents and Chemotherapy,* 13**,** 637-640.

Tejamaya, M., Romer, I., Merrifield, R.C. & Lead, J.R., 2012. Stability of citrate, pvp, and peg coated silver nanoparticles in ecotoxicology media. *Environmental Science & Technology,* 46**,** 7011-7017.

Udekwu, K.I., Parrish, N., Ankomah, P., Baquero, F. & Levin, B.R., 2009. Functional relationship between bacterial cell density and the efficacy of antibiotics. *Journal of Antimicrobial Chemotherapy,* 63**,** 745-757.

Van Hyning, D.L., Klemperer, W.G. & Zukoski, C.F., 2001. Characterization of colloidal stability during precipitation reactions. *Langmuir,* 17**,** 3120-3127.

Van Hyning, D.L. & Zukoski, C.F., 1998. Formation mechanisms and aggregation behavior of borohydride reduced silver particles. *Langmuir,* 14**,** 7034-7046.

Vijayaraghavan, K. & Yun, Y.-S., 2008. Bacterial biosorbents and biosorption. *Biotechnology Advances,* 26**,** 266-291.

Von Moos, N., Bowen, P. & Slaveykova, V.I., 2014. Bioavailability of inorganic nanoparticles to planktonic bacteria and aquatic microalgae in freshwater. *Environmental Science: Nano,* 1**,** 214-232.

Von Moos, N. & Slaveykova, V.I., 2014. Oxidative stress induced by inorganic nanoparticles in bacteria and aquatic microalgae – state of the art and knowledge gaps. *Nanotoxicology,* 8**,** 605-630.

Wakshlak, R.B.-K., Pedahzur, R. & Avnir, D., 2015. Antibacterial activity of silver-killed bacteria: the "zombies" effect. *Sci. Rep.,* 5.

West, F.K., West, P.W. & Iddings, F.A., 1966. Adsorption of traces of silver on container surfaces. *Analytical Chemistry,* 38**,** 1566-1570.

Xiu, Z.-M., Zhang, Q.-B., Puppala, H.L., Colvin, V.L. & Alvarez, P.J.J., 2012. Negligible particle-specific antibacterial activity of silver nanoparticles. *Nano Letters,* 12**,** 4271-4275.

Xu, H.Y., Qu, F., Xu, H., Lai, W.H., Wang, Y.A., Aguilar, Z.P. & Wei, H., 2012. Role of reactive oxygen species in the antibacterial mechanism of silver nanoparticles on *Escherichia coli* O157:H7. *Biometals,* 25**,** 45-53.

Zhang, C., Hu, Z. & Deng, B., 2015. Silver nanoparticles in aquatic environments: Physiochemical behavior and antimicrobial mechanisms. *Water Research*.

Zhang, W., Crittenden, J., Li, K. & Chen, Y., 2012. Attachment efficiency of nanoparticle aggregation in aqueous dispersions: modeling and experimental validation. *Environmental Science & Technology,* 46**,** 7054-7062.

Table 1. Cell viability and dissolved Ag concentration (mean ± SD) after exposure to Ag^+ or AgNPs for 72 h.

Ag^+			AgNPs		
Treatment (μg/L)	Viable count ($\times 10^6$ CFU/mL)	Dissolved Ag (μg/L)	Treatment (μg/L)	Viable count ($\times 10^6$ CFU/mL)	Dissolved Ag (μg/L)
0	22.7 ± 1.5	N/A	0	0.82 ± 0.03	N/A
5	4.9 ± 0.2	0.19 ± 0.01	10	11.5 ± 0.3	0.10 ± 0.10
10	4.8 ± 0.2	0.10 ± 0.02	20	4.8 ± 0.2	0.05 ± 0.06
20	8.0 ± 0.9	0.18 ± 0.06	50	0	14.8 ± 0.5
30	0	8.4 ± 0.3	100	0	17.8 ± 0.2

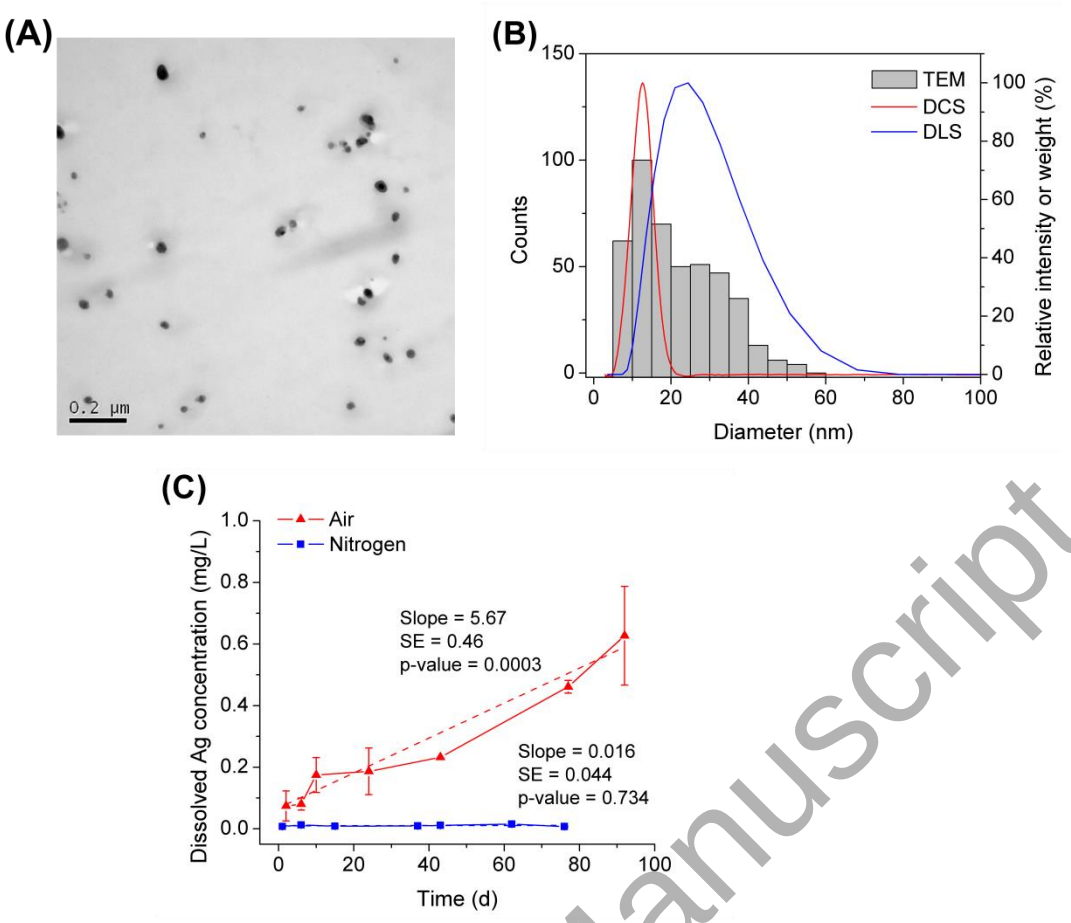

Figure 1. Characteristics of uncoated AgNPs. (A) Morphology of uncoated AgNPs by TEM. (B) Size distributions of the AgNP stock. The histogram of size distribution (n = 438) was obtained from TEM images analysed with ImageJ.(Schneider *et al.*, 2012) The size distributions measured by DLS and DCS show intensity and relative weight against diameter, respectively. (C) Stability of uncoated AgNPs stored under air or nitrogen. The total Ag concentration of AgNP stock under air or nitrogen was 25 and 2.3 mg/L, respectively. Error bars indicate standard deviations of at least two measurements.

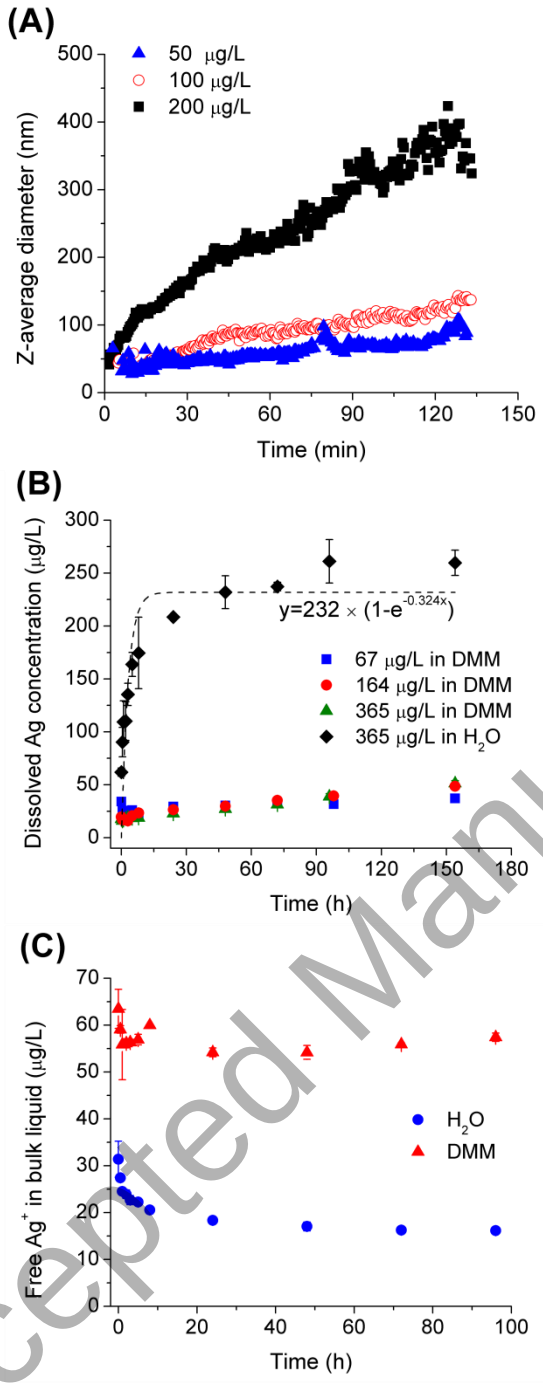

Figure 2. (A) Aggregation kinetics of AgNPs (50, 100 and 200 μg/L) in DMM salts solution. Hydrodynamic sizes (z-average size) were measured by real-time DLS. The polydispersity indeces (PDI) of the Z-average sizes showed no trends (Figure S5) and were 0.30 ± 0.08 (50 μg/L), 0.30 ± 0.10 (100 μg/L) and 0.27 ± 0.07 (200 μg/L) (mean ± SD). (B) Dissolution kinetics of AgNPs in H_2O or DMM salts solution. The volume loss due to evaporation at this temperature was calibrated to be 0.322 mL/d. Error bars indicate the standard errors of triplicates (n =3). (C) Adsorption kinetics of Ag^+ to a glass flask in H_2O or in DMM salts solution. The type of glass flasks, washing

procedures for glass flasks, volume of liquid and temperature were the same as for the dissolution kinetics experiment. Error bars indicate the standard errors of triplicates (n=3).

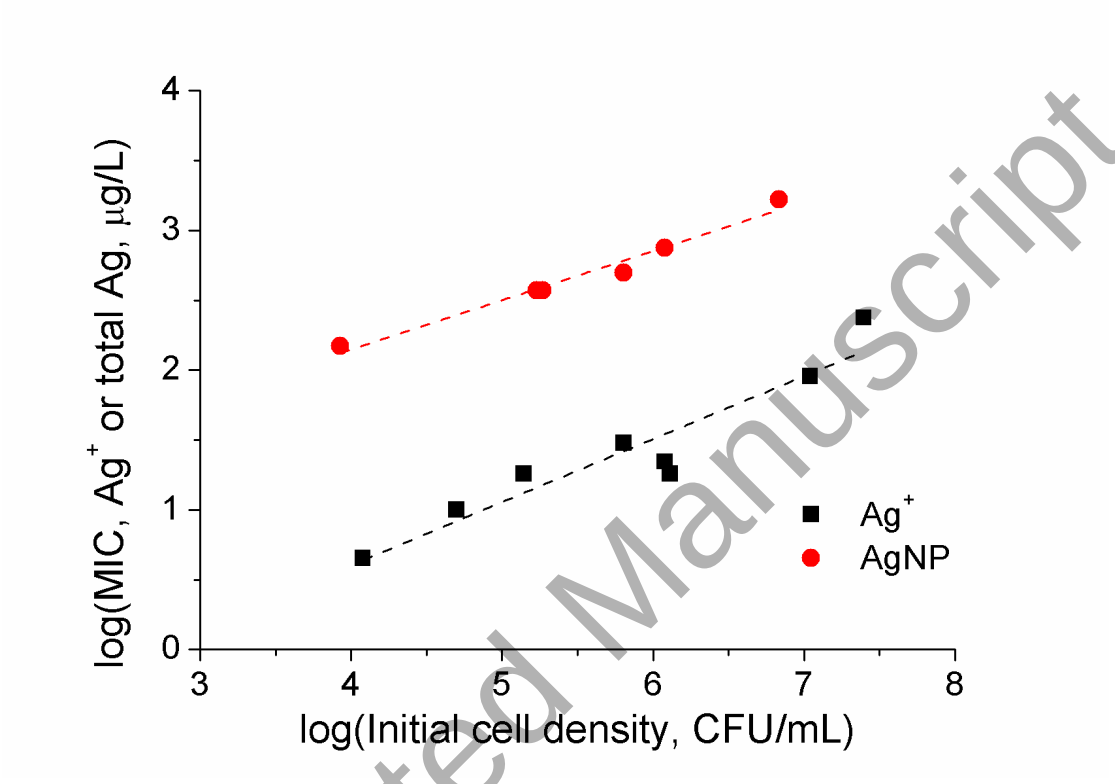

Figure 3. MICs of Ag^+ and AgNPs increased with initial cell densities. The MICs of AgNPs are shown as the total Ag concentration of AgNP suspensions. The relationship between the MICs of Ag^+ and AgNPs and initial cell densities appeared to follow a power law. Therefore, linear regression of log(MIC) versus log(Initial cell density) was carried out to infer the parameters of the power law. The p-values for the linear correlation of the log-transformed values were 4.0×10^{-4} and 2.7×10^{-4} for Ag^+ and AgNPs, respectively, suggesting that the power law is a suitable model. The slope of the linear regression (exponent of power law) was 0.45 ± 0.06 and 0.35 ± 0.03 (value ± SE) for Ag^+ and AgNPs, respectively. There was no significant difference between the two slopes (p-value = 0.19) based on a t-test using R (Version 3.3.3). The intercept of the linear regression was -1.20 ± 0.37 and 0.74 ± 0.16 (value ± SE) for Ag^+ and AgNPs, respectively. These two intercepts were significantly different (p-value = 4.8×10^{-4}) based on a t-test using R (Version 3.3.3).

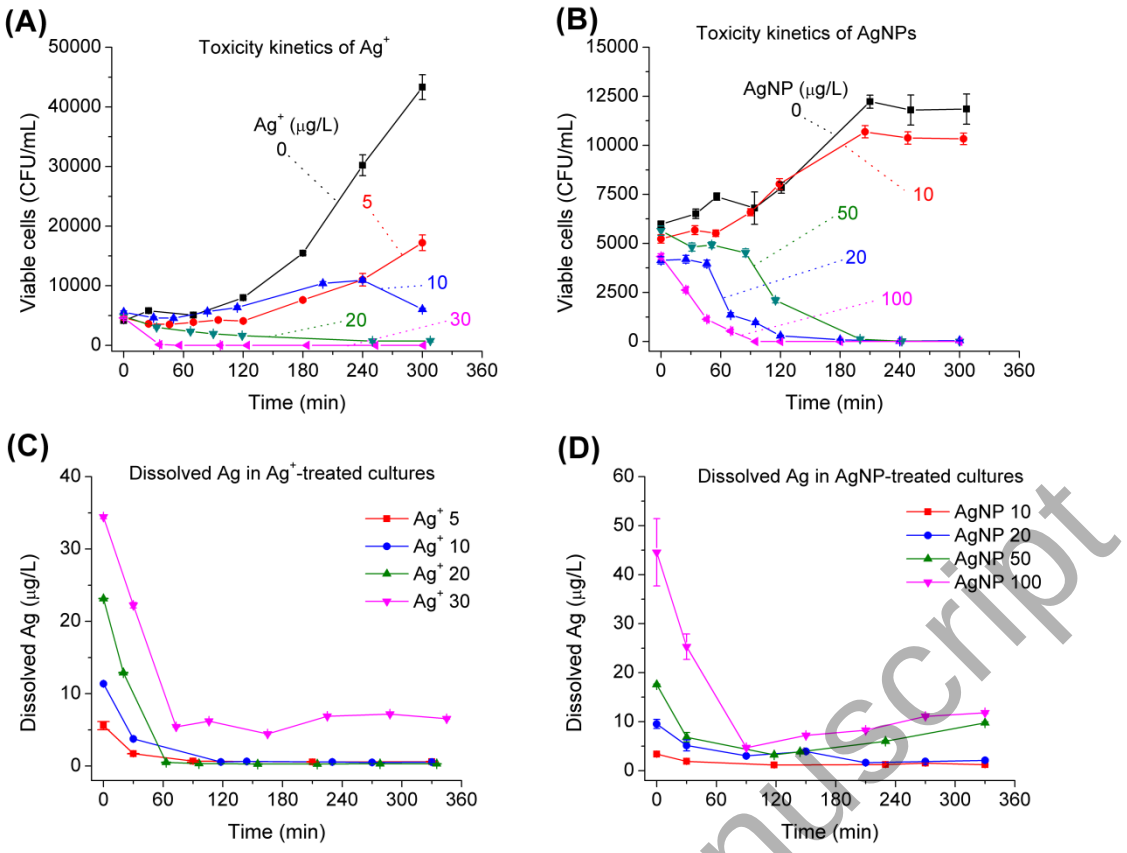

Figure 4. Toxicity kinetics of Ag^+ or AgNPs to *P. putida*. Viable cell counts for (A) Ag^+ treatment (0, 5, 10, 20 and 30 μg/L) or (B) AgNP treatment (0, 10, 20, 50 and 100 μg/L). Error bars represent the standard deviations of viable counts. Dissolved Ag concentrations in (C) Ag^+-treated cultures corresponding to panel A or in (D) AgNP-treated cultures corresponding to panel B. The error bars indicate standard deviations of triplicate measurements of each sample by GFAAS.

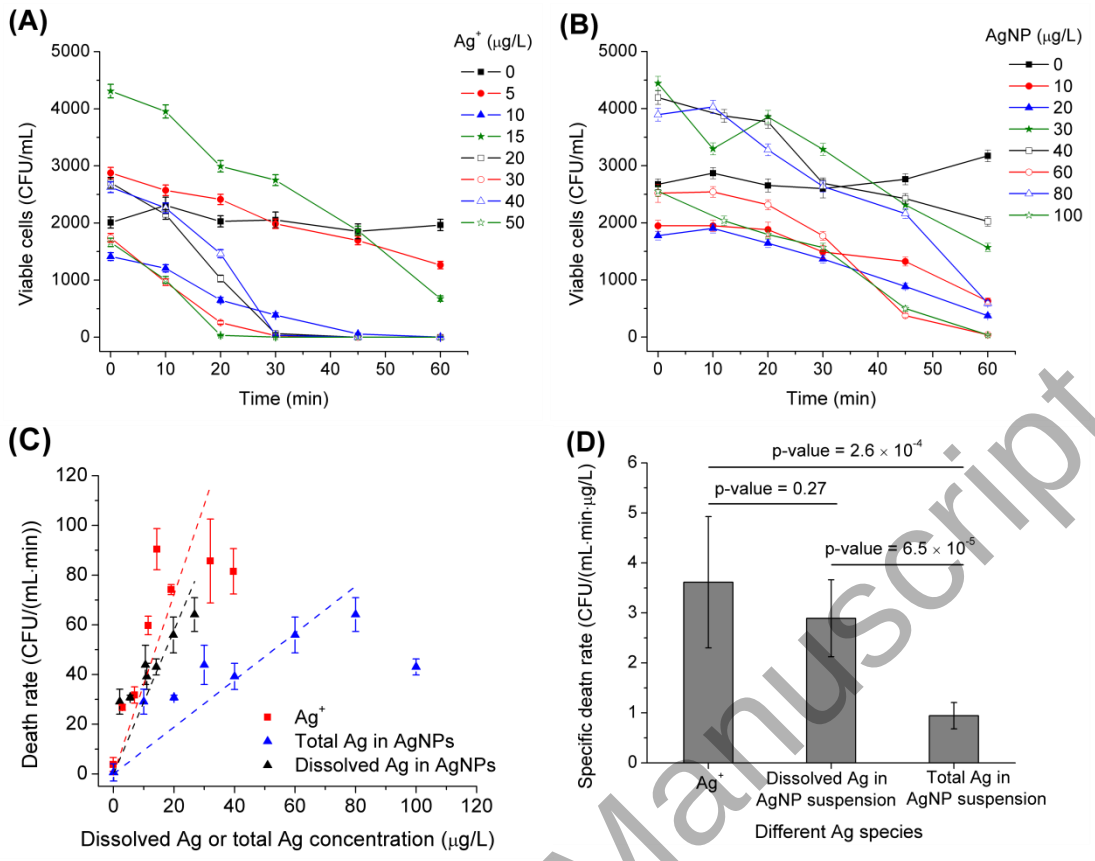

Figure 5. High-resolution inhibition kinetics for (A) Ag^+ and (B) AgNPs. Error bars indicate standard deviations of viable counts. (C) Death rate versus initial concentrations of Ag^+, dissolved Ag in AgNP suspensions or total Ag in AgNP suspensions. The death rates were calculated by linear regression of cell viability against time in the linear ranges shown in panel A and B, excluding counts of zero and lags were present. The error bars are standard errors of the regression slopes. (D) Specific death rates, defined as death rate per Ag concentration data in panel c (intercept = 0), within the range of 0–32 μg/L for Ag^+, 0–80 μg/L for total Ag in AgNPs and 0–27 μg/L for dissolved Ag in AgNPs. The error bars are 95% confidence intervals. The p-values for comparison of the three specific death rates were obtained with a t-test using R (Version 2.9.2).